# Theory of domain formation in inhomogeneous ferromagnetic dipolar condensates

Jay D. Sau,[1, 2, *] S. R. Leslie,[3] D. M. Stamper-Kurn,[3, 2] and Marvin L. Cohen[3, 2]

[1]*Department of Physics, University of Maryland,*

*College Park, Maryland 20742, USA*

[2]*Materials Sciences Division, Lawrence Berkeley*

*National Laboratory, Berkeley, California 94720, USA*

[3]*Department of Physics, University of California, Berkeley, California 94720, USA*

(Dated: October 29, 2018)

## Abstract

Recent experimental studies of $^{87}$Rb spinor Bose Einstein condensates have shown the existence of a magnetic field driven quantum phase transition accompanied by structure formation on the ferromagnetic side of the transition. In this theoretical study we examine the dynamics of the unstable modes following the transition taking into account the effects of the trap, non-linearities, finite temperature and dipole-dipole interactions. Starting from an initial state which includes quantum fluctuations, we attempt to make quantitative comparisons with recent experimental data on this system and estimate the contribution of quantum zero-point fluctuations to the domain formation. Finally, using the strong anisotropy of the trap, we propose ways to observe directly the effects of dipole-dipole interactions on the spinor condensate dynamics.

PACS numbers: 03.75.Mn

## I.   INTRODUCTION

The physics of phase transitions between ordered and disordered phases has been studied extensively in the past and has yielded answers to many fundamental questions about the effects of interactions and of quantum and thermal fluctuations on the equilibrium properties in various phases. However, because of the short time-scales and high levels of noise and impurities involved in traditional condensed matter systems, it has been difficult to study the *dynamics* of such transitions in detail. Ultra-cold atoms, because of their low densities and temperatures, provide an opportunity to study the non-equilibrium dynamics around phase transitions in a spatially and temporally resolved fashion. Bose Einstein condensates (BECs) of atoms with a spin degree of freedom, i.e. spinor BECs, are an example of such a system where it is possible to observe non-equilibrium spin dynamics and how they are affected by quantum noise and the proximity to phase transitions[1].

Recent experiments[1,2] have reported the formation of magnetic structures in ultra-cold spin-1 $^{87}$Rb gases. Spin-1 atoms support two characteristic families of quantum states: polar states exemplified by the $m_z = 0$ hyperfine state and magnetic states exemplified by the $m_z = \pm 1$ hyperfine state[3,4,5]; here $m_z$ denotes the eigenvalue for the dimensionless spin projection along the $\hat{z}$ axis. As discussed further below, spin-dependent contact interactions naturally favor the ferromagnetic state in $^{87}$Rb spinor condensates. The Rb atom may also be subjected to an extrinsic quadratic Zeeman shift, which lowers the energy of the $m_z = 0$ state by an amount $q$ with respect to the average of the energies of the $m_z = \pm 1$ states. In the experiments, a non-magnetic $m_z = 0$ condensate is prepared at a large value of $q$, where its internal state composition is stable. Following this, $q$ is rapidly quenched to a regime where the initially prepared $m_z = 0$ becomes unstable. As population flows to the initially unoccupied $m_z = \pm 1$ states, the condensed gas is observed to break translational and rotational symmetry spontaneously and form ferromagnetic domains of transversely magnetized atoms. In the experiment, the system also evolves under a significant linear Zeeman splitting of the three Zeeman sublevels $m_z = 0, \pm 1$. However, as we shall see later, since most of the terms of the Hamiltonian are invariant under global unitary spin rotations, the linear Zeeman shifts can be eliminated from the theoretical treatment by a global unitary transformation of the spin into the rotating frame of the Larmor precessing spin.

The symmetry-breaking ferromagnetic domain formation discussed above is a phe-

nomenon that accompanies a large number of thermodynamic phase transitions such as the paramagnetic to ferromagnetic phase transition seen in iron when the temperature is lowered below its Curie point. However, unlike the thermodynamic phase transition in Fe, the symmetry-breaking transition in the spinor BEC is a quantum transition that can occur at arbitrarily low temperature. Concomitantly, the initial fluctuations that seed the symmetry breaking dynamics in a spinor BEC need not be thermal in nature but, rather, may be of a quantum origin. The quantum origin of such fluctuations makes the detailed study of the origin and dynamics of the spontaneous magnetization of fundamental interest.

One approach to developing a theoretical understanding of the above phenomenon is to analyze the low energy dynamics of a spinor BEC by linearizing the Heisenberg equation of motion of the bosonic annihilation operators for the atoms. In previous theoretical studies[6,7], these linearized equations of motion were obtained by expanding the fields corresponding to the three components of the BEC around the initial $m_z = 0$ state. One finds that the low energy dynamics of the condensate in the initial state can be described by a set of three low energy excitations composed of a gapless phonon mode and two gapped magnon modes. On quenching the quadratic Zeeman shift to a value which is below the phase transition, the magnon modes are found to become unstable. These unstable modes amplify any initial perturbations from a homogeneous polar state. Thus the domain formation following the quench is described as resulting from the quantum fluctuations in the initial ground state being dynamically amplified[6,7].

The theoretical calculations discussed above treat the domain formation by calculating the linearized dynamics of a homogeneous spinor condensate with local interactions. While these calculations yield results in qualitative agreement with experiment, a quantitative comparison to experiment is essential for confirming the quantum nature of the initial seed and of the amplifier driving the structure formation. An improved understanding of the dynamics of the spinor condensate including the effect of the trapping potential and non-linearities has been obtained in previous theoretical works[7,8,9]. In the current work, we improve further our understanding of the dynamics of spinor condensates by including the effects of dipole-dipole interactions and finite temperature and use this improved understanding to determine the domain formation resulting from quantum fluctuations within the truncated Wigner approximation (TWA).

We begin with a discussion of how the condensate in a pancake-shaped trap can be

modeled by a two dimensional Hamiltonian. Next we introduce a general framework for calculating the eigenmodes of the inhomogeneous gas which are used to describe the time evolution of the initial quantum fluctuations. Following this we discuss explicitly the effect of dipole-dipole interactions, the trap and finite temperatures on the dynamics of a spinor BEC. Next we introduce the approximations and the general computational framework that allows us to include all these effects together with non-linearity effects such as saturation of the transverse magnetization at long times. Finally we comment on how our results compare to experimental results.

## II.   TWO-DIMENSIONAL EFFECTIVE HAMILTONIAN

The many-body Hamiltonian for the spin-1 $^{87}$Rb gas considered in this work, expressed using bosonic fields $\hat{\psi}_{m_p}$ to represent the three magnetic sublevels $m_p = 0, \pm 1$, is given as[8,10]

$$H = \int d\mathbf{R} \left\{ \frac{\hbar^2}{2M} \sum_\alpha |\nabla \hat{\psi}_\alpha|^2 + c_0(\hat{n}^2 - \hat{n}) + c_2 \hat{\mathbf{F}}^2 + q(t)\hat{Q} + V_{trap}(\mathbf{R})\hat{n} \right\} + U_{dipole} \quad (1)$$

where $M$ is the atomic mass, and the quadratic Zeeman shift, $q(t)$ is applied along $\mathbf{P}$ and $V_{trap}(\mathbf{R})$ is the external trap potential. The parameter $c_0$ is the strength of the spin-independent atom-atom short range repulsion, $c_2$ is the coupling constant for the spin-dependent contact interaction, and $U_{dipole}$ is the dipole-dipole interaction. The boson field operators appear in the magnetic part of the interaction terms through the spin density operators defined as $\hat{F}_\alpha = \sum_{\beta,\gamma} J_{\alpha,\beta,\gamma} \hat{\psi}_\beta^\dagger \hat{\psi}_\gamma$ where $J_\alpha$ are the spin-1 matrices in the fundamental representation in a basis such that the spin is quantized along $\mathbf{P}$, which is the axis determined by the quadratic Zeeman shift. The quadratic Zeeman shift term in the Hamiltonian is of the form $\hat{Q} = \sum_{\beta,\gamma} (\mathbf{P} \cdot J)_{\beta,\gamma}^2 \hat{\psi}_\beta^\dagger \hat{\psi}_\gamma$. The total atom density is given by $\hat{n} = \sum_\alpha |\hat{\psi}_\alpha|^2$. In the above discussion, the condensate is prepared in the $m_p = 0$ hyperfine state, where $m_p$ is the magnetic quantum number for spins quantized along the axis $\mathbf{P}$. This state is prepared at a high quadratic Zeeman shift $q(t) \gg 2|c_2|n_{3D}$ where $n_{3D}$ is the peak density at the center of the condensate. The quadratic Zeeman shift is then rapidly reduced below the critical value of $2|c_2|n_{3D}$ and the state of the condensate is allowed to evolve. In the experimental work discussed in this paper the axis along which the quadratic Zeeman shift is applied $\mathbf{P}$ is taken to be the z-axis.

As mentioned in the introduction, the atoms in the system evolve under a strong magnetic

field which we have eliminated from the Hamiltonian described in Eq. 1, by transforming to a rotating frame. Such a transformation leaves the rotation-invariant terms in the Hamiltonian unchanged but affects the quadratic Zeeman shift term and the dipole-dipole interaction term $U_{dipole}$. Yet, under the experimental conditions that the Larmor precession frequency is far higher than that of the interaction-driven spin dynamics, one may consider the quadratic Zeeman shift term and the dipole interaction as precession-averaged static terms in the Hamiltonian. It may also be possible to vary dynamically the axis of the quadratic Zeeman shift to follow the Larmor precession of the initial state applied by the initial magnetic field, in which case the quadratic Zeeman shift term would be intrinsically stationary in the rotating frame of the spin.

The above defined Hamiltonian can be used to calculate the dynamics of the transverse magnetization, which is the observed quantity that is used in the above mentioned experimental studies to observe the non-magnetic to ferromagnetic phase transition[1]. The $x$ and the $y$ components of the transverse magnetization, $\hat{F}_x$ and $\hat{F}_y$, can be combined into a single complex transverse magnetization operator $\hat{F}_\perp(\mathbf{R}) = \hat{F}_x(\mathbf{R}) + \hat{F}_y(\mathbf{R})$ which is given in terms of the fields $\hat{\psi}_\alpha$ by

$$\hat{F}_\perp(\mathbf{R}) = \sqrt{2}\left(\hat{\psi}_0^\dagger(\mathbf{R})\hat{\psi}_{+1}(\mathbf{R}) + \hat{\psi}_0(\mathbf{R})\hat{\psi}_{-1}^\dagger(\mathbf{R})\right) \tag{2}$$

The random magnetization domain pattern that forms after the quench can be characterized by a correlation function of the above defined transverse magnetization, which we take as $G(\delta\mathbf{R}) = \int d\mathbf{R} \left\langle \hat{F}_\perp(\mathbf{R} - \delta\mathbf{R}/2)\hat{F}_\perp^\dagger(\mathbf{R} + \delta\mathbf{R}/2)\right\rangle / \left(\int d\mathbf{R} \left\langle \hat{n}(\mathbf{R})\right\rangle\right)^2$ [1].

An important feature of the experiments is the use of condensates with widths in one dimension ($\hat{y}$) that are smaller than the spin healing length, $2\pi/\sqrt{2M|c_2|n_{3D}}$. The three-dimensional Hamiltonian is thus reduced to a two dimensional form through the substitutions $\hat{\psi}_\alpha(\mathbf{R}) = \hat{\phi}_\alpha(\mathbf{r})\xi(\mathbf{r};y)\sqrt{n_{2D}}$ where $y = \mathbf{R} \cdot \hat{y}$ and $\mathbf{R} = \mathbf{r} + y\hat{y}$. The peak density integrated along the $y$ axis is given by $n_{2D} = \int dy \left\langle \hat{n}(0,y)\right\rangle_{initial}$. Here $\xi(\mathbf{r};y)$ represents the normalized spatial profile of the wavefunction at each point $\mathbf{r}$ in the two dimensional $x$-$z$ plane. The scale of the initial quantum zero-point fluctuations of the two dimensional field, $\hat{\phi}_\alpha$, is determined from the canonical commutation relations $[\hat{\phi}_\alpha(\mathbf{r}), \hat{\phi}_\beta^\dagger(\mathbf{r}')] = \frac{1}{n_{2D}}\delta(\mathbf{r} - \mathbf{r}')\delta_{\alpha,\beta}$.

Using these relations and the Heisenberg equations of motion one can construct a time-

evolution equation for the operator $\hat{\phi}_\alpha(\mathbf{r})$ of the form

$$\imath\partial_t\hat{\phi}_\alpha(\mathbf{r}) = \left(-\frac{\hbar^2}{2M}\right)\nabla_{\mathbf{r}}^2\hat{\phi}_\alpha(\mathbf{r}) + \hat{\phi}_\alpha(\mathbf{r})\int \mathrm{d}y\,\left(-\frac{\hbar^2}{2m}\right)\left(\nabla^2\xi(\mathbf{r};y)\right)\xi(\mathbf{r};y)$$

$$+\,\hat{\phi}_\alpha(\mathbf{r})\int \mathrm{d}y\,\xi^2(\mathbf{r};y)V_{trap}(\mathbf{r};y) + U_{interaction} \tag{3}$$

The second term on the right hand side of the above equation may be considered to be an effective renormalization of the potential energy related to confinement effects. Within the Thomas-Fermi (TF) approximation this term is small through most of the condensate and is hence ignored.

For simplicity, we assume the wavefunction profile to be a TF profile given by $\xi(\mathbf{r};y) = \frac{3}{4R_{\mathrm{TF},y}(\mathbf{r})}(1 - y^2/R_{\mathrm{TF},y}^2(\mathbf{r}))^{1/2}$ where $R_{\mathrm{TF},y}(\mathbf{r}) = R_{\mathrm{TF},y}(1 - x^2/R_{\mathrm{TF},x}^2 - z^2/R_{\mathrm{TF},z}^2)^{1/2}$ and $R_{\mathrm{TF},x}$, $R_{\mathrm{TF},y}$ and $R_{\mathrm{TF},z}$ are the TF radii in the $x$, the $y$ and the $z$ directions respectively. With the above choice of a transverse profile, the contribution of a local two-body potential of the form $c_m\delta(\mathbf{r}-\mathbf{r}')\delta(y-y')$ to the interaction term $U_{interaction}$ simplifies to

$$c_m\int \psi^3(\mathbf{R})\xi(\mathbf{r};y)\,\mathrm{d}y = c_m\frac{n_{3D}}{|\xi(\mathbf{0})|^2}\int \xi^4(\mathbf{r};y)\,\mathrm{d}y\,\phi^3(\mathbf{r}) = 0.8\,c_m n_{3D}\frac{R_{\mathrm{TF},y}(\mathbf{0})}{R_{\mathrm{TF},y}(\mathbf{r})}\phi^3(\mathbf{r}) \tag{4}$$

where the index $m$ is either 0 or 2 depending on whether we are referring to the spin independent or spin dependent parts of the contact interaction, respectively. In the rest of the article we will be using a two-dimensional position-dependent effective interaction by $c_m(\mathbf{r}) = 0.8\,c_m n_{3D}R_{\mathrm{TF},y}(\mathbf{0})/R_{\mathrm{TF},y}(\mathbf{r})$.

## III.   QUANTUM DYNAMICS AND QUANTUM NOISE SEEDED DOMAIN FORMATION

Let us now describe the fluctuations and domain formation in terms of the two dimensional fields derived above. We consider the dynamics and low energy fluctuations of the initial $m_p = 0$ state by shifting the operator corresponding to the $m_p = 0$ component by $\hat{\phi}_0 = \sqrt{n(\mathbf{r})} + \hat{\eta}_0$, where $n(\mathbf{r}) = \langle\hat{\phi}_0^\dagger(\mathbf{r})\hat{\phi}_0(\mathbf{r})\rangle$ is the equilibrium density for the condensate at large positive quadratic Zeeman shift of $q \gg |c_2|n_{3D}$. The Hamiltonian can now be expanded to second order in the small fluctuations in the small fluctuation operators $\hat{\phi}_{\pm 1}, \hat{\eta}_0$. In this Hamiltonian, the terms involving $\hat{\eta}_0$, which describe the scalar Bogoliubov spectrum of phonons and free particles, separate from those involving spin excitations; these latter

6

terms provide the following Hamiltonian

$$
\begin{aligned}
H_{magnon} = {}&{-}\frac{\hbar^2}{2M} \int \hat{\phi}^{\dagger}_{+1}\nabla^2\hat{\phi}_{+1} + \hat{\phi}^{\dagger}_{-1}\nabla^2\hat{\phi}_{-1} \\
&+ \int \left( q(t) + c_2(\mathbf{r})n(\mathbf{r}) + V_{trap}(\mathbf{r}) + c_0(\mathbf{r})n(\mathbf{r}) \right) \left( \hat{\phi}^{\dagger}_{+1}\hat{\phi}_{+1} + \hat{\phi}^{\dagger}_{-1}\hat{\phi}_{-1} \right) \\
&+ \int c_2(\mathbf{r})n(\mathbf{r}) \left( \hat{\phi}_{+1}\hat{\phi}_{-1} + \hat{\phi}^{\dagger}_{+1}\hat{\phi}^{\dagger}_{-1} \right).
\end{aligned}
\tag{5}
$$

For simplicity, the effect of the dipole-dipole interaction term has been ignored here and its discussion is postponed to Section V. The dynamics of the magnetic degrees of freedom obtained from the above approximate Hamiltonian are given as

$$
\partial_t\hat{\Phi}(\mathbf{r}) = \left\{ \imath \left( -\frac{\hbar^2}{2M}\nabla^2 + q(t) + V_{trap}(\mathbf{r}) + (c_0(\mathbf{r}) + c_2(\mathbf{r}))n(\mathbf{r}) \right) \sigma_z + c_2 n(\mathbf{r})\sigma_y \right\} \hat{\Phi}(\mathbf{r}).
\tag{6}
$$

where we have introduced the spinor $\hat{\Phi}(\mathbf{r}) = \begin{pmatrix} \hat{\phi}_{+1}(\mathbf{r}) \\ \hat{\phi}^{\dagger}_{-1}(\mathbf{r}) \end{pmatrix}$.

The above spinor equation of motion can be used to describe the dynamics of the condensate in terms of normal modes $\Upsilon_n^{(\pm 1)}(\mathbf{r})$ with frequencies $\pm E_n$. The dynamics of $\hat{\Phi}(\mathbf{r}, t)$ are then determined as

$$
\hat{\Phi}(\mathbf{r}, t) = \sum_{n,\sigma=\pm 1} \hat{d}_n^{(\sigma)} e^{\imath\sigma E_n t} \Upsilon_n^{(\sigma)}(\mathbf{r}).
\tag{7}
$$

where $\hat{d}_n^{(\sigma)}$ are the mode occupancy operators. The magnon modes are stable when the eigenenergies $E_n$ are real, and unstable when $E_n$ are complex. It is these unstable modes that amplify quantum fluctuations to generate macroscopic magnetization in the quenched spinor gas.

In the case of a homogeneous condensate the normal modes $\Upsilon_n^{(\pm 1)}(\mathbf{r})$ can be reduced to a product of a plane wave state and the momentum dependent two-component spinor that appears in standard treatments of the linearized Gross-Pitaevskii equations. However the determination of these modes in the case of an inhomogeneous density must be done in real space using explicit numerical diagonalization of a generalized eigenvalue problem. In the case of a positive quadratic shift, which is the focus of in this article, the frequencies of these eigenmodes can be shown to be either purely real or imaginary as discussed in Appendix A. A similar eignmode expansion for a trapped spinor condensate in the limit of vanishing quadratic Zeeman shift has been reported in previous work[7].

The quantum noise amplified by these unstable modes is entirely contained in the correlation function of the spinors relative to the initial state. Since the initial state of our

system is assumed to be prepared as a condensate of atoms in the $m_p = 0$ state, the population in the $m_p = \pm 1$ states is negligible and the relevant correlator is given by $\left\langle \hat{\Phi}(\mathbf{r}_1, 0)\hat{\Phi}^\dagger(\mathbf{r}_2, 0) \right\rangle = \delta(\mathbf{r}_1 - \mathbf{r}_2)(1 + \sigma_z)/2$. In the description of the dynamics of the condensate in terms of magnon modes, the quantum fluctuations become encoded in the quantum mode occupancy operators $\hat{d}_n^{(\sigma)}$, which can be derived from the spinor operator at the time of quench $\hat{\Phi}(\mathbf{r}, 0)$, $\hat{d}_n^{(\sigma)} = \int d\mathbf{r} \, \tilde{\Upsilon}_n^{(\sigma)*}(\mathbf{r})\hat{\Phi}(\mathbf{r}, 0)$, where $\tilde{\Upsilon}_n^{(\sigma)}(\mathbf{r})$ are the dual modes, explicit expressions for which can be found in Appendix A.

Given this initial noise and the linear dynamics of these magnon modes, we may calculate the magnetization correlations that may be observed at short times after the quench. Linearizing the transverse magnetization as $\hat{F}_\perp(\mathbf{r}) = n_{2D}\sqrt{2n(\mathbf{r})}\left(\hat{\phi}_{+1}^\dagger(\mathbf{r}) + \hat{\phi}_{-1}(\mathbf{r})\right)$, we obtain

$$
G(\delta\mathbf{r}) = \frac{\int d\mathbf{r}\langle\hat{F}_\perp(\mathbf{r} - \delta\mathbf{r}/2)\hat{F}_\perp^\dagger(\mathbf{r} + \delta\mathbf{r}/2)\rangle}{\left(\int d\mathbf{r}\, n_{2D}n(\mathbf{r})\right)^2} = \sum_{n,m,\sigma,\sigma'} e^{\iota(\sigma E_n - \sigma' E_m^*)t}
$$

$$
\times \frac{\int d\mathbf{r}\sqrt{n(\mathbf{r} - \delta\mathbf{r}/2)n(\mathbf{r} + \delta\mathbf{r}/2)}\,\Upsilon_m^{(\sigma')\dagger}(\mathbf{r} - \delta\mathbf{r}/2)(\mathbf{1} + \sigma_x)\Upsilon_n^{(\sigma)}(\mathbf{r} + \delta\mathbf{r}/2)}{\left(\int d\mathbf{r}\, n(\mathbf{r})\right)^2}
$$

$$
\times \int d\mathbf{r}_1\,\tilde{\Upsilon}_n^{(\sigma)\dagger}(\mathbf{r}_1)(\mathbf{1} + \sigma_z)\tilde{\Upsilon}_m^{(\sigma')}(\mathbf{r}_1) \tag{8}
$$

Note that the correlation function defined above suffers from a UV divergence. The physical origin of this divergence is the fact that $\hat{F}_\perp$ represents the magnetization of point-like particles. This UV divergence is however not observed experimentally because of the physically natural cut-offs like the finite spatial and temporal resolution of the measuring apparatus, which introduces a natural spatio-temporal averaging into the observed magnetization. For our purposes it suffices to consider only the contribution of unstable magnon modes to the transverse magnetization. Hence in our calculations we avoid this UV divergence in the correlator of $\hat{F}_\perp$ by restricting the above sum to imaginary frequency modes.

## IV.  NON-LINEARITY EFFECTS: TRUNCATED WIGNER APPROXIMATION

In the last section we saw how we can describe the physics of the quench by expanding the Heisenberg equations of motion about the initial condensate state and keeping terms up to linear order in the fluctuations. Even though this might be expected to be a relatively accurate description at short times where deviations from the initial state are small, it breaks down at longer times and predicts an unphysical diverging magnetization.

Such a divergence is avoided by considering the complete Hamiltonian, including the higher order terms neglected in our prior approximation. The direct solution of the Heisenberg equations of motion with the non-linearity terms would present an extremely difficult task. This is a general feature of problems involving quantum many-particle systems and for this reason various approximations must be used to understand such problems. One such approximation, that has been seen to describe the dynamics of BECs reasonably well[11], is the Truncated Wigner Approximation (TWA)[12,13].

Within the TWA one is interested in calculating the time evolution of the Wigner Distribution Function (WDF) of the fields $\hat{\phi}_\sigma(\mathbf{r})$, which are the quantum analog of the classical phase space distribution. The fields are assumed to evolve according to the Gross-Pitaevskii equation (GPE) which is the mean field version of the Heisenberg equation of motion where the operator $\hat{\phi}_\sigma(\mathbf{r})$ has been replaced by the time-dependent order parameter $\phi_\sigma(\mathbf{r})$. Quantum fluctuations around the mean field time evolution are included in the TWA by adding to the initial condition of the order parameter a noise term which is picked randomly from a classical distribution of fields corresponding to the initial WDF. In our case, where the initial state has a negligible population in the $m_p = \pm 1$ hyperfine state, the classical distribution of the randomly picked wavefunctions, $\phi_\sigma(\mathbf{r})$, is a Gaussian distribution with variance given by $\langle \phi_\sigma^*(\mathbf{r})\phi_{\sigma'}(\mathbf{r'})\rangle_{classical} = \frac{1}{2}\langle \Psi_{initial}|\{\hat{\phi}_\sigma^\dagger(\mathbf{r})\hat{\phi}_{\sigma'}(\mathbf{r'})\}|\Psi_{initial}\rangle$ where $|\Psi_{initial}\rangle$ is the initial state with all atoms in the $m_p = 0$ hyperfine state.[27].

Within the TWA, we obtain the magnetization correlation function by averaging over numerical results obtained for the different, random representations of quantum noise. As shown in Fig. 1, this procedure yields a satisfactory result for the magnetization variance $G(\mathbf{0})$ that saturates rather than diverging.

The TWA has been shown to describe dynamical phenomena in BECs with reasonable success. However the TWA fails to describe certain aspects of the dynamics of BECs, such as the non-condensate fraction, and improvements beyond the TWA have been proposed in several works[14,15]. It is difficult to estimate the accuracy of the TWA in the full multi-mode spinor condensate system that we are studying. However as has been observed in previous work[10], it is possible to solve the Hamiltonian under consideration within the single mode approximation exactly. This corresponds to the limit of a small trap where we can ignore the spatial dependence of the dynamics of the atoms completely and the system of $2N$ atoms can be described by a Hamiltonian given by $\hat{H}_{SMA} = (2N - \hat{\phi}_0^\dagger\hat{\phi}_0)(\hat{\phi}_{+1}^\dagger\hat{\phi}_{+1} + \hat{\phi}_{-1}^\dagger\hat{\phi}_{-1}) - (\hat{\phi}_{+1}^\dagger\hat{\phi}_{-1}^\dagger\hat{\phi}_0^2 +$

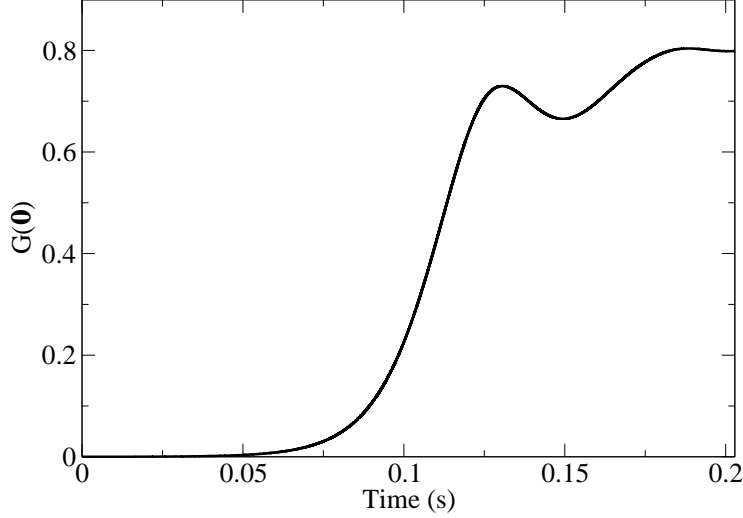FIG. 1: Evolution of the variance of the transverse magnetization for the experimental configuration[2] for $q/h = 2$ Hz and $c_2(\mathbf{0})/h = 8$ Hz, calculated using the TWA to include non-linearity induced saturation effects.

$\hat{\phi}_0^{\dagger 2} \hat{\phi}_{+1} \hat{\phi}_{-1}$). The time evolution of the fluctuations in the transverse magnetization of this Hamiltonian can be determined exactly by numerically solving the time evolution of an initial state where all atoms are in the $m_p = 0$ hyperfine state. We compared the results of this calculation for a system of 2000 atoms to the time evolution of the transverse magnetization obtained within the TWA for the same system and found excellent agreement between the growth rate within the TWA to exact results up to the saturation time within the TWA. The exact transverse magnetization was found to increase past the saturation value within the TWA to a value that was 10% higher than the TWA saturation. While it is possible that the multimode non-linearity of our system causes physics beyond the TWA to become directly relevant, the above comparisons of the TWA to exact results for the single mode systems demonstrate that the TWA accounts for some of the effects of non-linearity in these systems.

## V.   FINITE TEMPERATURE EFFECTS FROM AN INITIAL PHONON POPULATION

In attempting to make quantitative comparisons between calculations and experimental observations, it is imperative to consider the role of the non-zero temperature on the initial

preparation and later evolution of the experimental system. In fact, at first glance, one might expect the quench experiments reported to be wholly dominated by thermal effects, given that the gas is prepared by evaporative cooling at a temperature of $T \approx 50$ nK for which the thermal energy is far larger than the spin-dependent energies responsible for the quench dynamics, i.e. $k_B T \gg |c_2| n_{3D}$. However, one must consider separately the *kinetic* and *spin* temperatures of the paramagnetic condensate in these experiments. While the thermal population of the scalar excitations, the $m_p = 0$ Bogoliubov excitations about the $m_p = 0$ condensate is indeed determined by the $T = 50$ nK kinetic temperature of the gas, the magnon excitations are expelled from the gas by the application of magnetic field gradients that purify the $m_p = 0$ atomic population. To the extent that such state purification is effective, and that magnon excitations are not thermally produced, e.g. by incoherent spin-exchange collisions, the initial *spin* temperature of the system is indeed near zero. Thus remarkably, a purely quantum evolution may indeed occur in the non-zero temperature gas.

Here, we consider the possible influence of the thermal population of scalar excitations on the quantum quench experiments. The study of the coupling of phonons and magnons requires going beyond the linearized Heisenberg equation of motion. Thus, we consider the time evolution operator for the quantum state of the spinor condensate as a coherent state path integral $U(t_1, t_2) = \int \prod_\alpha D\phi_\alpha D\phi_\alpha^* \exp(\imath S[\phi_\alpha, \phi_\alpha^*])$, as has been found useful for many boson problems[16]. Here $S$ is the action for the three-component boson field corresponding to the Hamiltonian in Section II. The scalar phonon fluctuations are composed of a scalar density fluctuation, $\delta n(\mathbf{r}, t) = \sum_\alpha |\phi_\alpha(\mathbf{r}, t)|^2 - n(\mathbf{r})$, and current fluctuations associated with the density fluctuations, required by number conservation. In the case of a condensate with population dominantly in the $m_z = 0$ hyperfine state, the current fluctuations can be described by the superfluid phase $\lambda(\mathbf{r}, t)$ defined through $\phi_0(\mathbf{r}, t) = e^{\imath \lambda(\mathbf{r}, t)} \sqrt{n(\mathbf{r}) + \delta n(\mathbf{r}, t) - |\phi_{+1}(\mathbf{r}, t)|^2 - |\phi_{-1}(\mathbf{r}, t)|^2}$. Since the density fluctuations are gapped at a high energy by the term $c_0 \delta n(\mathbf{r}, t)^2 / 2$ in the action $S$, they can be integrated out to leave an effective action involving the phase $\lambda(\mathbf{r}, t)$. Therefore in order to eliminate the high frequency density fluctuations we perform the field substitution $\phi_{\pm 1}(\mathbf{r}, t) \to \phi_{\pm 1}(\mathbf{r}, t) e^{\imath \lambda(\mathbf{r}, t)}$ in the action $S$ and then integrate out the density fluctuations $\delta n(\mathbf{r}, t)$. This leads to the approximate action $S_{approx} = S_{phonon}[\lambda] + S_{magnon}[\phi_{\pm 1}] + V_{coupling}[\phi_{\pm 1}, \lambda]$ where the $S_{phonon} = n\dot{\lambda}^2 / 2c_0 + n\frac{\hbar^2}{2M}(\nabla\lambda)^2$, $S_{magnon}$ is the usual action for the $\phi_{\pm 1}$ atoms without the scalar interaction term and $V_{coupling} = \frac{\hbar^2}{2M}[-\nabla\lambda \cdot \sum_\alpha \text{Im}(\phi_\alpha \nabla \phi_\alpha^*)]$. The last term is the

interaction that describes the coupling between phonons and magnons.

The non-zero kinetic temperature of the gas gives causes (low frequency) fluctuations of superfluid phase with variance given by $\langle|\lambda_k|^2\rangle = 2Mk_BT/\hbar^2k^2n_{2D}$. These thermal phase fluctuations couple to the dynamics of the magnons, through the interaction term $V_{coupling}$. A rough estimate of the magnitude of the effect of the kinetic temperature can be made by considering the dimensionless ratio of the r.m.s value of $V_{coupling}$ to the spin mixing energy $|c_2|n$ which is given by $\sqrt{\hbar^2k_{spin}^2/2M}\sqrt{(k_BT)k_{phonon}^2/n_{2D}}/|c_2|n_{3D} \approx \sqrt{(2Mk_BT)|c_2|/\hbar^2n_{2D}c_0}$ where $k_{spin}$ is the wavevector associated with the spin healing length and $k_{phonon}$ is the small wavevector associated with a phonon at the energy scale of the spin dynamics, $|c_2|n_{3D}$. For the kinetic temperature in experiment of 50 nK, this dimensionless parameter characterizing thermal effects is found to be less than $1.3 \times 10^{-2}$. A more rigorous calculation within the TWA, where phonons are introduced by adding random thermal fluctuations to the initial conditions in $\phi_0$, confirms our rough estimate by showing a negligible effect of the kinetic temperature.


## VI.  ROLE OF DIPOLE-DIPOLE INTERACTIONS

In the preceding paragraphs we have discussed the physics of the formation of domains from quantum fluctuations in a trapped quasi-two-dimensional condensate with ferromagnetic interactions. However theoretical[17,18] and experimental studies[19] suggest that dipolar interactions play an important role in determining the magnetization textures for this system. In this section, we provide the first characterization of the role of dipolar interactions on the quantum quench dynamics of a $^{87}$Rb spinor BEC.

The atomic spin undergoes Larmor precession at a high frequency, on the order of tens of kHz, even as slower dynamics responsible for spontaneous magnetization transpire. While this Larmor precession has no influence on average on the spin dependent s-wave contact interaction or the quadratic Zeeman shift, the time averaged Larmor precession of the atoms must be accounted for in calculating the influence dipolar interactions, yielding an effective precession-averaged interaction of the form[20,21]

$$U_{dipole} = \frac{\mu_0}{8\pi}(g_F\mu_B)^2 \int d\mathbf{R}_1\, d\mathbf{R}_2\, \frac{(\mathbf{R}_1 - \mathbf{R}_2)^2 - 3(\mathbf{D} \cdot (\mathbf{R}_1 - \mathbf{R}_2))^2}{|\mathbf{R}_1 - \mathbf{R}_2|^5}$$
$$[3(\mathbf{D} \cdot \hat{\mathbf{F}}(\mathbf{R}_1))(\mathbf{D} \cdot \hat{\mathbf{F}}(\mathbf{R}_2)) - \hat{\mathbf{F}}(\mathbf{R}_1) \cdot \hat{\mathbf{F}}(\mathbf{R}_2)] \tag{9}$$

where $\mathbf{D}$ is the dipole-precession axis (the magnetic field axis), $g_F = 1/2$ is the gyromagnetic ratio of the electron, $\mu_B$ is the Bohr magneton. Integrating over the thin dimension of the condensate, we derive an effective two-dimensional dipole interaction as

$$U_{dipole} = \frac{c_{dd}}{2} \int d\mathbf{r_1}\, d\mathbf{r_2}\, K(\mathbf{r_1}, \mathbf{r_2})[3(\mathbf{D} \cdot \hat{\mathbf{F}}(\mathbf{r}_1))(\mathbf{D} \cdot \hat{\mathbf{F}}(\mathbf{r}_2)) - \hat{\mathbf{F}}(\mathbf{r}_1) \cdot \hat{\mathbf{F}}(\mathbf{r}_2)] \qquad (10)$$

$$K(\mathbf{r}, \mathbf{r}') = \frac{1}{\xi^2(\mathbf{0})} \int \frac{(\mathbf{R} - \mathbf{R}')^2 - 3(\mathbf{D} \cdot (\mathbf{R} - \mathbf{R}'))^2}{|\mathbf{R} - \mathbf{R}'|^5} \xi^2(\mathbf{r}; y)\xi^2(\mathbf{r}'; y')\, dy\, dy' \qquad (11)$$

where the dipole interaction strength is given by $c_{dd} = \frac{n_{3D}\mu_0}{4\pi}(g_F\mu_B)^2$. The dipole-dipole interaction term $U_{dipole}$ is a spin-dependent interaction term in the Hamiltonian in addition to the ferromagnetic part of the contact interaction already discussed. The total of the two spin-dependent parts of the interaction Hamiltonian is given by

$$H_{spin} \equiv \int d\mathbf{r}\, c_2(\mathbf{r})\hat{\mathbf{F}}(\mathbf{r})^2 + U_{dipole} = \int d\mathbf{r}_1\, d\mathbf{r}_2\, c_2^{\text{eff}}(\mathbf{r_1}, \mathbf{r_2}) \frac{[\hat{\mathbf{F}}(\mathbf{r}_1) \cdot \hat{\mathbf{F}}(\mathbf{r}_2)]}{\sqrt{n(\mathbf{r}_1)n(\mathbf{r}_2)}}$$
$$+ \frac{3}{2} \int d\mathbf{r}_1\, d\mathbf{r}_2\, c_{dd}K(\mathbf{r_1}, \mathbf{r_2})(\mathbf{D} \cdot \hat{\mathbf{F}}(\mathbf{r_1}))(\mathbf{D} \cdot \hat{\mathbf{F}}(\mathbf{r_2})) \qquad (12)$$

$$c_2^{\text{eff}}(\mathbf{r_1}, \mathbf{r_2}) = c_2(\mathbf{r_1})n(\mathbf{r_1})\delta(\mathbf{r_1} - \mathbf{r_2}) - c_{dd}\sqrt{n(\mathbf{r_1})n(\mathbf{r_2})}K(\mathbf{r_1}, \mathbf{r_2})/2 \qquad (13)$$

Thus apart from renormalizing the spin-dependent part of the contact interaction to $c_2^{\text{eff}}$, the dipole-dipole interaction also has an intrinsically anisotropic contribution which is given by the second term in Eq. 12, where the anisotropy is not related to the spatial anisotropy of the dipole interaction kernel $K$. This term however turns out to not be relevant for the linearized dynamics in the case where the dipole precession axis $\mathbf{D}$ coincides with the spin-quantization axis $\mathbf{P}$.

In the homogeneous case $c_2^{\text{eff}}$ can be written as below

$$c_2^{\text{eff}}(k, \chi, \eta) = c_2(\mathbf{0}) - \frac{c_{dd}}{2}K(k, \chi, \eta) \qquad (14)$$

where $K(k, \chi, \eta)$ is the dipole interaction kernel, and $\chi$ is the angle that $\mathbf{D}$ makes with the $y$-axis and $\eta$ is the polar angle of the vector $\mathbf{D}$ in the plane of the BEC, as shown in Fig. 2. The wave-vector $k$ is taken to be along the $z$-axis in the plane of the BEC. As discussed in Appendix A, the eigenmode treatment discussed in Section III can be easily generalized to include dipole-dipole interactions.

From Eq. 14 it is apparent that in the three-dimensional homogeneous case dipole-dipole interactions enhance structure formation for wave-vectors along the dipole-precession axis
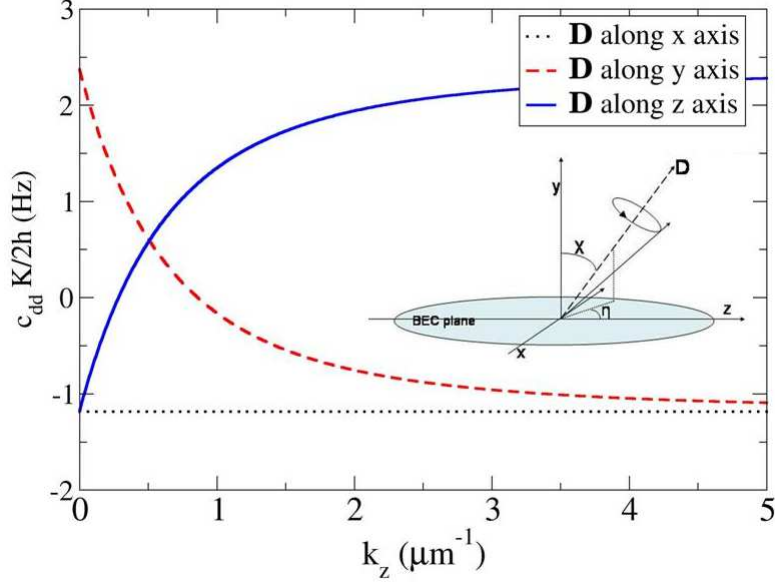
13

FIG. 2: Momentum dependence of the contribution of the dipole interaction kernel K defined in Eq. 15 to $c_2^{\text{eff}}$ for $c_{dd}/h = 0.8$ Hz, $c_2(\mathbf{0})/h = -8.0$ Hz. The inset shows the orientation of the dipole-precession axis $\mathbf{D}$ relative to the coordinates and the plane of the BEC.

and suppress it for wave-vectors transverse to the dipole-precession axis. However the effect of dipole-dipole interactions on a quasi-two-dimensional condensate is qualitatively different. The Fourier transform of the interaction $K(k, \chi, \eta)$ in the case of the parabolic TF transverse profile along the $y$ direction is difficult to compute analytically. To obtain a qualitative understanding of dipole interactions we consider the case of a 2D condensate for the case of a Gaussian profile $\xi(\mathbf{r}; y)$ of width $w = \frac{4}{3\sqrt{2\pi}} R_{\text{TF},y}$. This width is chosen so that the peak density for the normalized profile matches that of the TF profile. The expression used for the Gaussian regularized dipole interaction derived in the Appendix B can be used in conjunction with standard integrals to determine the Fourier transform of $K(\mathbf{r})$ for this Gaussian choice of profile to be

$$K(k, \chi, \eta) = \sqrt{2\pi} \left[ \frac{4\sqrt{\pi}}{3} (1 - \frac{3}{2} \sin^2 \chi) + \pi k w (\sin^2 \chi \cos 2\eta + 3 \sin^2 \chi - 2)(1 - \text{Erf}(kw)) e^{k^2 w^2} \right].$$
(15)

The contribution of the momentum variation of the dipole interaction kernel $K$ to $c_2^{\text{eff}}$ is shown in Fig. 2. In the large $k$ limit, this expression, apart from a factor of $\sqrt{2}$ arising from the re-normalization because of the transverse profile, reduces to $-\frac{4\pi}{3}(1 - 3\sin^2 \chi \cos^2 \eta)$ which is the three dimensional form as expected. As seen in Fig. 2, the small $k$ limit is
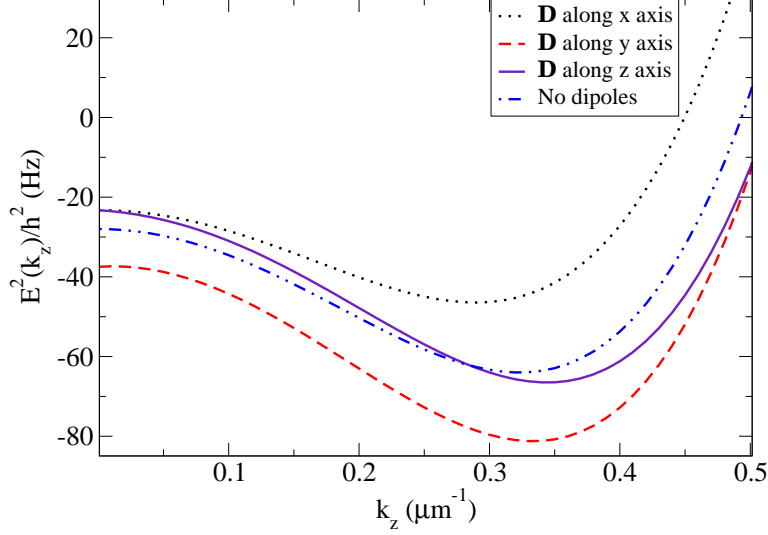
14

FIG. 3: Magnon dispersion curves for an unbounded two-dimensional condensate in the $x - z$ plane, for $q/h = 2$ Hz, $c_2(\mathbf{0})/h = 8$ Hz and $c_{dd}/h = 0.8$ Hz, including the effects of dipole-dipole interaction for $\mathbf{D}$ aligned along $\hat{\mathbf{x}}$, $\hat{\mathbf{y}}$ or $\hat{\mathbf{z}}$, and the wave-vector being assumed to be aligned along $\hat{\mathbf{z}}$.

found to be consistent with previous theoretical studies[21].

In the case where the dipole-precession axis $\mathbf{D}$ coincides with the spin-quantization axis of the atoms $\mathbf{P}$, we can use the explicit form for $c_2^{\text{eff}}$ given in Eq. 14 to discern the effect of the anisotropic dipole-dipole interactions on behavior of the spin dynamics by studying the dispersion relation $E^2(\mathbf{k}) = (\frac{\hbar k^2}{2M} + q)(\frac{\hbar k^2}{2M} + q + 2c_2^{\text{eff}}(\mathbf{k}))$ in the presence of dipole-dipole interactions. As seen in Fig. 3, when the dipole-precession axis points along the long axis of the condensate, i.e the $z$-axis, as in the experiments, the effect of the dipole interaction is weak and the dipole interactions slightly shorten the length scale and lengthen the time scale of domain formation. In contrast, the domain formation is significantly slowed down by the dipole-dipole interaction when $\mathbf{D}$ is oriented along the $x$-direction. Interestingly when the dipole axis is pointed along the $y$-axis, the thin axis of the condensate, the rate of structure formation is dramatically increased in both directions.

The effects of the anisotropic dipolar interactions may also be highlighted in quantum quenches where the dipole-precession axis $\mathbf{D}$ differs from the spin-quantization axis $\mathbf{P}$. Specifically, consider the case where $\mathbf{D} = \hat{y}$, while $\mathbf{P}$ is prepared to be orthogonal to $\mathbf{D}$ (i.e. the axis $\mathbf{P}$ Larmor precesses in the $\hat{x} - \hat{z}$ plane). In this case the intrinsic spin-anisotropic term in Eq. 12 can no longer be ignored when constructing the linearized dynamics of a

two-dimensional homogeneous condensate and this leads to a contribution which breaks the symmetry of the two polarizations of the magnon modes describing the magnetization dynamics of the condensate. Altogether the strong variation of post-quench dynamics with changes in the system geometry provides a compelling signature of dipole-dipole interactions that may be studied in future experiments.

## VII.   NUMERICAL METHODS AND RESULTS

Having set up our theoretical model we now turn to the numerical techniques and quantitative results based on these ideas applied to a model spinor condensate with parameters motivated from experiment. As previously discussed, the calculation of correlation functions within the TWA requires the time evolution of an initial state which is comprised of an initial mean field state with random fluctuations added to it. The initial wavefunction of the $m_z = 0$ condensate is determined by minimizing the total energy via conjugate gradient minimization assuming $q \to \infty$. Time evolution according to the GPE is determined numerically by the 6-th order Runge Kutta method[22] with periodic boundary conditions in space. The kinetic energy is computed by Fourier transforming each component into momentum space. The dipole-dipole interaction kernel, $K(\mathbf{r}, \mathbf{r}')$, has the properties both of being long-ranged and also of being singular at short distances. Therefore it is necessary to regularize and truncate $K(\mathbf{r}, \mathbf{r}')$ in real space before calculations are performed in Fourier space to avoid interaction between inter-supercell periodic images as discussed in Appendix B. In calculating $K(\mathbf{r}, \mathbf{r}')$ for use in the solution of the full GPE, we neglect the variation of the condensate thickness ($R_{TF,y}$) along the $\hat{x}$ direction. We have checked that this approximation doesn't significantly affect our results when $\mathbf{D}$ is along the long axis of the trap i.e. $\hat{z}$, as is the case in experiment.

For the calculations reported we use a time step of $3.5\,\mu$s and a grid spacing of $0.5\,\mu$m and the results are found to be converged with respect to these parameters. In addition, the total energy of the system remains conserved to a certain error tolerance in the time evolution. It is also verified that the total magnetization along $\mathbf{D}$ is a conserved quantity in the absence of dipole-dipole interactions.

The trap geometry for our calculations is taken to be similar to experiment[2] such that the TF radii of the condensate are $R_{\mathrm{TF},x} = 20\,\mu$m, $R_{\mathrm{TF},y} = 1.6\,\mu$m. Given that the relevant

lengthscale for spin dynamics $(2\pi/\sqrt{2M|c_2|n_{3D}} \approx 2\mu\text{m})$ is much smaller than the $\hat{z}$ length of the condensate $(R_{TF,z} = 200\,\mu\text{m})$, here we treat the system as unconfined along $\hat{z}$, with periodic boundary conditions over a 90 $\mu$m length. The peak three-dimensional and two-dimensional densities are taken to be $n_{3D} = 2.5 \times 10^{14}/\text{cm}^3$ respectively. The strength of the spin-dependent part of the contact interaction has been inferred previously from molecular spectroscopy[23,24] and from spin-mixing dynamics[25,26]. According to these works $c_2(\mathbf{r} = 0) = 0.8\,|c_2|n_{3D}$ is predicted to lie between $h \times 6$ Hz and $h \times 8$ Hz, corresponding to $1.1\,a_B < \Delta a = (a_0 - a_2) < 1.9\,a_B$ where $\Delta a$ is the difference between the $s$-wave scattering lengths for the spin-0 and spin-2 channels and $a_B$ is the Bohr radius. This variation in the rate of spin-amplification makes it difficult to estimate how close the estimated initial noise from experiment is to the quantum limit.

We find our results to be in qualitative agreement with experiment and previous theoretical calculations. In particular, we find that the average magnitude of the transverse magnetization grows exponentially from a small value to a much larger value (Fig. 1) with a time-constant that is relatively insensitive to the quadratic Zeeman shift $q$. The calculated domain structure and magnetization correlations match with those observed experimentally, and in previous calculations[9], the characteristic domain size increasing with $q$ (Fig. 4). However as seen from Fig. 5 our calculations somewhat underestimate the domain size for the larger of the experimentally measured values of $\Delta a$. This discrepancy between theory and experiment is reduced on using the smaller of the measured values of $\Delta a$. Thus the difference between theory and experiment could be the result of an error in the experimentally measured value of the spin-dependent contact interaction or quantum and thermal effects of interactions that are not contained in the Gross-Pitaevskii equations. The introduction of a dipole-dipole interaction introduces a weak dependence of the average local transverse magnetization $G(\mathbf{0})$ on the quadratic Zeeman shift.

Despite the qualitative agreement between the homogeneous 2D condensate calculation[6] and the current results, we find quantitative differences between the results of the homogeneous case and the calculations including the trap and dipole interactions that are important for comparison to experiment. We discuss several of these differences below.
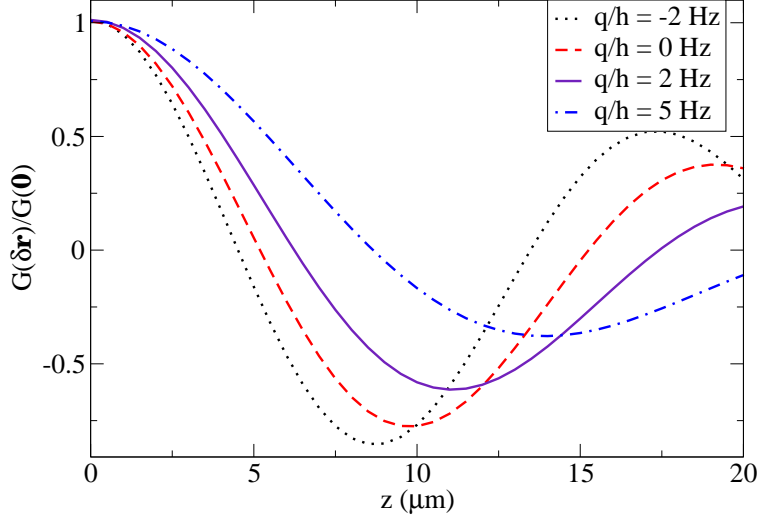
FIG. 4: Correlation function $G(\delta \mathbf{r} = z\hat{\mathbf{z}})$ at $t = 100$ ms for a spinor condensate calculated using the method and geometry described in Section VII for various quadratic Zeeman shifts. The correlation function plotted along the length of the condensate shows decreasing domain size with decreasing quadratic Zeeman shift.

## A. Effect of the trapping potential

Similar to previous theoretical work[7], we find a significant effect of the inclusion of the trap on the spin dynamics in the parameter regime corresponding to experiment. The external trapping potential along the width of the condensate, which is accounted for in our numerical calculations, is found to slow the growth of the transverse magnetization in the condensate significantly as seen in Fig. 7, when compared to the quasi-two-dimensional homogeneous case without a trapping potential along the width. This slowing down can be understood intuitively from the fact that the trap causes the density away from the center of the trap to be lower than at the center of the trap. Consistent with previous theoretical work[7], the density reduction away from the center of the trap also affects the spatial structure of the correlations observed and the trap is found to suppress the formation of structure in the radial direction, as seen in Fig. 5.
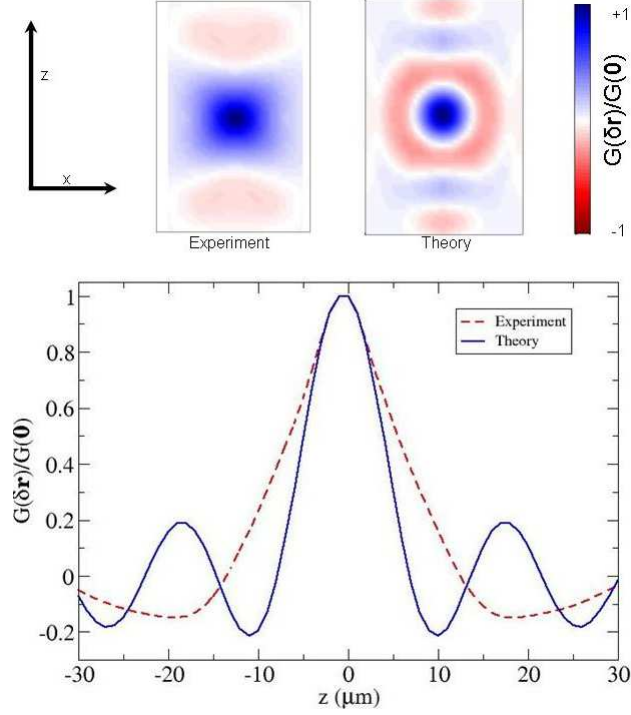
FIG. 5: Planar correlation function $G(\delta\mathbf{r})$ at $t = 87$ ms for a spinor condensate calculated using the method and geometry described in Section VII for $q/h = 2$ Hz. The one dimensional plots shown in the lower half represent sections of the two dimensional plots above through the center of the condensate at $x = 0$. The two dimensional plots are 100 $\mu m$ along the $z$ direction and 40 $\mu m$ along the $x$ direction. The above plots compare the calculated correlation structure on the left to the experimentally measured structure on the right[2].

## B. Effect of the dipole interaction

As discussed in Section VI, dipole-dipole interactions reduce the rate of domain formation in the case where the magnetic field is aligned along the $z$-direction, which is the long axis of the condensate. However, as seen in Fig. 5, for the parameters of the calculation, which are taken to be the ones relevant to experiment, the effect of the dipole-dipole interaction on the average transverse magnetization $G(\mathbf{0})$ turns out to be small because the Fourier transform of the dipole interaction kernel $K$ almost vanishes at the lengthscale of domain formation. That is, the spin healing length being nearly equal to the narrower condensate thickness, the dominant length scale for domain formation coincides with the cross-over between the 2D and 3D forms of the dipole interaction. Despite having a negligible effect
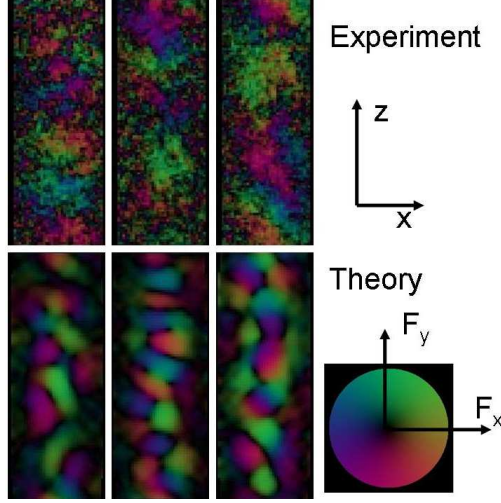
FIG. 6: Spatial structure of the complex transverse magnetization $F_\perp(\mathbf{r})$ in the $x - z$ plane at $t = 87$ ms for $q/h = 2$ Hz. The upper panel of figures consist of random instances of experimentally measured spin textures[2] while the lower figures are random instances of calculated spin textures. Each figure in the panel is 100 $\mu$m long and 40 $\mu$m wide. The complex number $F_\perp$ is represented as shown in the color wheel in the inset of the figure. Domains are seen to have limited structure along the width of the trap and localized at the center of the condensate.

on domain formation in the longitudinal direction, dipole-dipole interactions are found to suppress domain formation along the radial direction.

Yet as discussed in Section VI, other experimental geometries, i.e. orientations of $\mathbf{D}$ and $\mathbf{P}$ away from the $z$ axis, are expected to show more prominent dipolar effects in the spontaneous formation of magnetization. We explored this possibility numerically. The magnitude of the magnetization variance $G(\mathbf{0})$ indicated by such calculations is shown in Fig. 6. One can see that the rate of growth of transverse magnetization is significantly enhanced with $\mathbf{D}$ and $\mathbf{P}$ pointing along the $y$-direction compared to other orientations.

## VIII. CONCLUSION

In our analysis we have studied a realistic quantum Hamiltonian model for a quasi-two dimensional spinor condensate, including the effects of the trap and dipole-dipole interactions, in order to make a quantitatively accurate prediction of the contribution of intrinsic fluctuations to the symmetry-breaking domain formation. Similar to previous studies, the inclusion
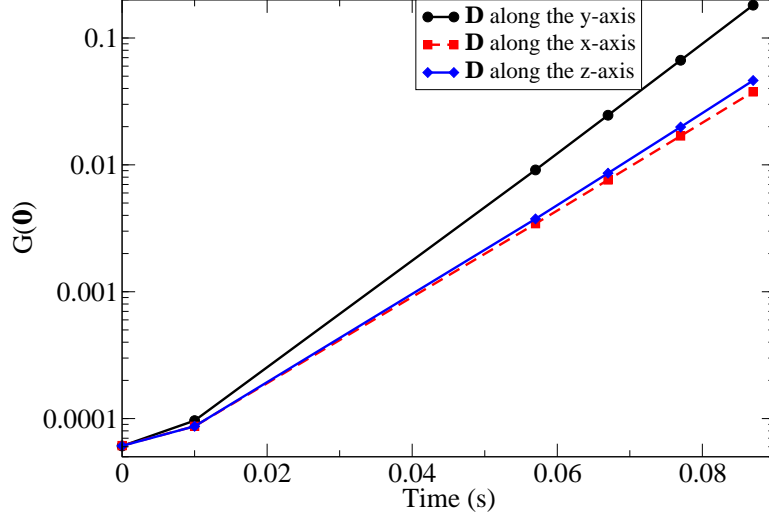
FIG. 7: Dependence of the evolution of the variance of the transverse magnetization for the dipole-precession axis $\mathbf{D}$ aligned along $\hat{\mathbf{x}}, \hat{\mathbf{y}}$ and $\hat{\mathbf{z}}$ directions for $q/h = 2.0$ Hz. The growth rate of transverse magnetization is found to be enhanced significantly for $\mathbf{D}$ aligned along $\hat{\mathbf{y}}$ as compared to $\mathbf{D}$ aligned along $\hat{\mathbf{z}}$ which yields results close to the case without dipole interaction.

of the trapping potential was found to reduce the rate of structure formation because of a reduction of the average density. The dipole-dipole interaction, which is known to have a dominant effect on the long term structure formation in spinor BECs, was found to add an effective non-local contribution to the spin-dependent part of the interaction in the spinor condensate. The non-local nature of the spin-spin interactions couples the spin structure formation dynamics to the direction of the spin polarization. Even though dipole-dipole interactions are found to affect the spin dynamics weakly when $\mathbf{D}$ and $\mathbf{P}$ are polarized along $m_z = 0$, we find that dipole interactions significantly enhance the rate of domain formation when these vectors are polarized along $m_y = 0$. Moreover, dipole-dipole interactions were found to split the degeneracy of the two polarizations of the magnon modes in the case where $\mathbf{D}$ was orthogonal to $\mathbf{P}$. This spin-polarization dependence of the domain formation rate leads to a direct way to observe experimentally the role of dipole-dipole interaction on spinor dynamics.

A quantitative prediction of the magnitude of the structure formation also requires the inclusion of effects from non-linear interaction terms and thermal effects. On a preliminary examination one would have expected thermal effects to be significant since the kinetic temperature of the condensate is much larger than the spin-mixing energy scale. However
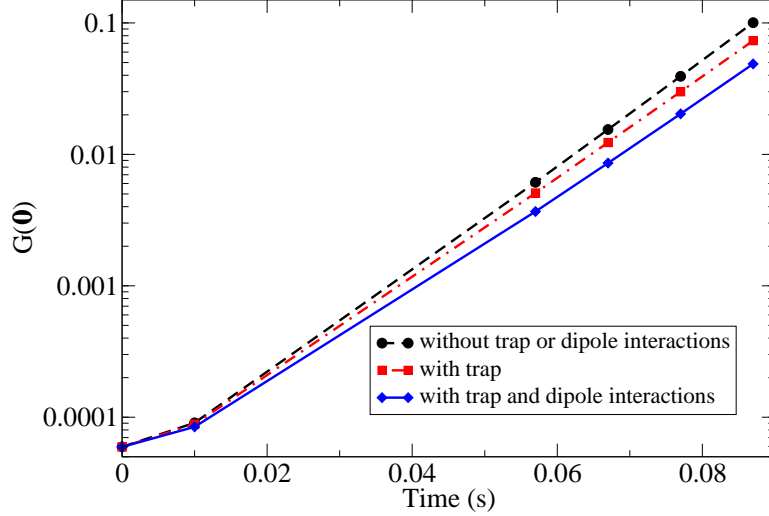
FIG. 8: Summary of effects of various factors on the evolution of the magnitude of transverse magnetization. Both dipole-dipole interactions and the external trapping interaction are found to reduce the growth rate of the transverse magnetization.

we found that the coupling of phonons to spin fluctuations is small, leading to a separation of the low temperature spin dynamics from the high temperature phonon dynamics. In Section IV, we studied the effects of the non-linear interactions within the standard TWA and found that non-linearity effects lead to saturation of the transverse magnetization at long times. We expect the TWA to be a reasonably accurate description of the spin-spin correlations of a spinor BEC since it was found to yield results in good agreement with exact diagonalization calculations our spinor BEC model in the single mode regime.

Despite our effort to include the effects of the trapping potential, dipole-dipole interactions, non-linearities and finite temperature to develop a quantitative understanding of the magnitude of domain formation, we found in Section VII that the uncertainty in the magnitude of the spin-dependent part of the contact interaction prevents us from making a quantitative comparison of the magnitude of the domain formation with experimental results. Such a quantitative comparison between theory and experiment is critical for the determination of the contribution of intrinsic quantum fluctuations to the domain formation. One possible experimental approach to resolving this problem is to determine in a direct way the gain of the spinor BEC in the experimental geometry by studying the dynamics of the magnetization of the condensate following an initial microwave pulse. Such experiments in conjunction with quantitative calculations might make it possible to determine better the

22

importance of intrinsic quantum fluctuations to symmetry breaking dynamics.

## APPENDIX A: EIGENMODES FOR THE BOGOLIUBOV TRANSFORMATION OF INHOMOGENEOUS DIPOLAR CONDENSATES.

Here we give explicit expressions for the eigenmodes and eigenfrequencies of a dipolar ferromagnetic spinor BEC for positive quadratic Zeeman shifts. As discussed in Section VI, the inclusion of dipole-dipole interactions requires the generalization of the local spin-dependent coupling constant $c_2 n$ to $c_2^{\text{eff}}(\mathbf{r_1}, \mathbf{r_2})$. The eignmodes and eigenfrequencies that we define are strictly valid when the Hermitean Hamiltonian $H_0 = -\frac{\hbar^2}{2M}\nabla^2 + q(t) + \mu + c_0 n(\mathbf{r}) + V_{trap}$ is positive definite. In this case the eigenmodes of the condensate are given by

$$\Upsilon_{+1}^{(\sigma n)}(\mathbf{r}) = \sigma E_n^{-1} H_0^{1/2} \xi_n(\mathbf{r}) \tag{A1}$$

$$\Upsilon_{-1}^{(\sigma n)}(\mathbf{r}) = H_0^{-1/2} \xi_n(\mathbf{r}). \tag{A2}$$

where $E_n^2$ and $\xi_n$ are defined to be eigenvectors and eigenvalues of the Hermitean operator $H_0^{1/2}(H_0 + 2c_2^{\text{eff}})H_0^{1/2}$ and $\sigma = \pm 1$. The dual modes then follow to have the form

$$\tilde{\Upsilon}_{+1}^{(\sigma n)}(\mathbf{r}) = \sigma E_n H_0^{-1/2} \xi_n(\mathbf{r}) \tag{A3}$$

$$\tilde{\Upsilon}_{-1}^{(\sigma n)}(\mathbf{r}) = H_0^{1/2} \xi_n(\mathbf{r}). \tag{A4}$$

In the case of negative quadratic Zeeman shifts, such a Hermitean eigenproblem cannot be constructed since some of the frequencies in this case are neither purely real nor imaginary. This can be verified by introducing a weak periodic potential to the homogeneous ferromagnetic Bose gas and diagonalizing the problem using degenerate perturbation theory.

## APPENDIX B: REGULARIZING THE DIPOLE POTENTIAL

In order to perform numerical calculations, even semi-analytic calculations where the Fourier transform of the three-dimensional dipole interaction kernel, $K(\mathbf{R} - \mathbf{R'}) =$

$\frac{(\mathbf{R}-\mathbf{R}')^2 - 3(\mathbf{D}\cdot(\mathbf{R}-\mathbf{R}'))^2}{|\mathbf{R}-\mathbf{R}'|^5}$, is needed, one needs the integral involved in the Fourier transform of the kernel to be well defined. The full 3D Fourier transform of the dipole interaction kernel may be calculated analytically, but to obtain converged results for the spin dynamics it is necessary to truncate the long-ranged dipole interaction between periodic images of the system which emerge when using Fourier techniques to do such calculations. For numerical convenience we imagine that the dipole density can be expanded in terms of a possibly overcomplete set of functions i.e

$$\phi(\mathbf{R}) = \frac{\sum_n \phi(\mathbf{R}_n^{(grid)})\rho(\mathbf{R} - \mathbf{R}_n^{(grid)})}{\sum_n \rho(\mathbf{R}_n^{(grid)})}. \tag{B1}$$

Such an expansion allows us to represent a function $\phi(\mathbf{R})$ which is smooth on the scale of the width of $\rho(\mathbf{R})$ by its value $\phi(\mathbf{R}_n^{(grid)})$ on a discrete grid of points $\mathbf{R}_n^{(grid)}$ with a grid spacing that is smaller than the width of $\rho(\mathbf{R})$. Integrals of the kernel $K(\mathbf{R})$ of interest are given by

$$\int \phi(\mathbf{R}_1)\phi(\mathbf{R}_1)K(\mathbf{R}_1 - \mathbf{R}_2) = \sum_{n_1,n_2} \frac{\phi(\mathbf{R}_{n_1}^{(grid)})\phi(\mathbf{R}_{n_2}^{(grid)})}{(\sum_n \rho(\mathbf{R}_n^{(grid)}))^2} \tag{B2}$$

$$\int d\mathbf{R}_1'\, d\mathbf{R}_2' \rho(\mathbf{R}_1' - \mathbf{R}_1)\rho(\mathbf{R}_2' - \mathbf{R}_2)K(\mathbf{R}_1 - \mathbf{R}_2). \tag{B3}$$

Taking the smoothing function to be $\rho(\mathbf{R}) = \frac{1}{w^3(2\pi)^{(3/2)}}e^{-R^2/2w^2}$, the averaged kernel $g$ is given by

$$g(\mathbf{R}) = \int d\mathbf{R}_1 d\mathbf{R}_2\, \rho(\mathbf{R}_1 - \mathbf{R})\rho(\mathbf{R}_2)K(\mathbf{R}_1 - \mathbf{R}_2) = \frac{(3\cos^2(\theta) - 1)}{R^3} \tag{B4}$$

$$\left[\mathrm{Erf}\left(\frac{R}{2w}\right) - \frac{R}{w\sqrt{\pi}}e^{-\frac{R^2}{4w^2}}\left(\frac{R^2}{6w^2} + 1\right)\right] \tag{B5}$$

The regularized expression, unlike the original dipole interaction kernel $K(\mathbf{R})$, vanishes for small $R$ and approaches the regular expression $\frac{(3\cos^2(\theta)-1)}{R^3}$ for large $R$ as expected.

Using the regularized kernel $g(\mathbf{R})$, the dipole interaction can be calculated on a real-space grid with grid spacings smaller than the width of the smoothing profile $\rho(\mathbf{R})$, in a way so as to avoid interaction between periodic images. The Fourier transform for the two dimensional kernel with a Gaussian profile given Eq. 15 in Section VI can be derived by applying a Fourier transform to $g(\mathbf{R})$ restricted to the 2D plane.

---

* Electronic address: jaydsau@umd.edu

[1] L. Sadler, J. Higbie, S. Leslie, M. Vengalattore, and D. M. Stamper-Kurn, Nature **443**, 312 (2006).

[2] S. Leslie, J. Guzman, M. Vengalattore, J. D. Sau, M. L. Cohen, and D. M. Stamper-Kurn, PRA(in press) (2008).

[3] T. L. Ho, Phys. Rev. Lett. **81**, 742 (1998).

[4] T. Ohmi and K. Machida, J. Phys. Soc. Jpn. **67**, 1822 (1998).

[5] R. Barnett, A. Turner, and E. Demler, Phys. Rev. Lett. **97**, 180412 (2006).

[6] A. Lamacraft, Phys. Rev. Lett. **98**, 160404 (2007).

[7] G. I. Mias, N. R. Cooper, and S. M. Girvin, Physical Review A **77**, 023616 (2008).

[8] H. Saito, Y. Kawaguchi, and M. Ueda, Phys. Rev. A **75**, 013621 (2007).

[9] H. Saito, Y. Kawaguchi, and M. Ueda, Phys. Rev. A **76**, 043613 (2007).

[10] H. Pu, C. Law, S. Raghavan, J. H. Eberly, and N. Bigelow, Phys. Rev. A **60**, 1463 (1999).

[11] M. T. Johnsson and S. A. Haine, Phys. Rev. Lett. **99**, 010401 (2007).

[12] A. A. Norrie, R. J. Ballagh, and C. W. Gardiner, Phys. Rev. A **73**, 043617 (2006).

[13] C. W. Gardiner and P. Zoller, *Quantum Noise* (Springer-Verlag, Berlin-Heidelberg, 2000).

[14] A. Polkovnikov, Phys. Rev. A **68**, 053604 (2003).

[15] P. Deuar and P. D. Drummond, Phys. Rev. Lett. **98**, 120402 (2007).

[16] S. Sachdev, *Quantum Phase Transitions* (Cambridge University Press, Cambridge, 2000).

[17] S. Doniach and T. Garel, Phys. Rev. B **26**, 325 (1982).

[18] K. De'Bell, A. B. MacIssac, and J. P. Whitehead, Rev. Mod. Phys. **72**, 225 (2000).

[19] M. Vengalattore, S. R. Leslie, J. Guzman, and D. M. Stamper-Kurn, Phys. Rev. Lett. **100**, 170403 (2008).

[20] Y. Kawaguchi, H. Saito, and M. Ueda, Phys. Rev. Lett. **98**, 110406 (2007).

[21] R. W. Cherng and E. Demler, arxiv **0806.1991** (2008).

[22] W. H. Press, S. A. Teukolsky, W. T. Vetterling, and B. P. Flannery, *Numerical Recipes: The art of scientific computing* (Cambridge University Press, Cambridge, 2007).

[23] N. N. Klausen, J. L. Bohn, and C. H. Greene, Phys. Rev. A **64**, 053602 (2001).

[24] E. G. M. van Kempen, S. J. J. M. F. Kokkelmans, D. J. Heinzen, and B. J. Verhaar, Phys. Rev. Lett. **88**, 093201 (2002).

[25] A. Widera, F. Gerbier, S. Folling, L. Gericke, O., and I. Bloch, New Journal of Physics **8**, 152 (2006).

[26] M. Chang, Q. Qin, W. Zhang, L. You, and M. S. Chapman, Nature Physics **1**, 111 (2005).

[27] To see this we observe that the requirement of equality of the quantum and the classical distributions is equivalent to the equality of the quantum characteristic function $\chi_W(\lambda, \lambda^*) = \langle \exp(\hat{\phi}^\dagger \lambda - \lambda^\dagger \hat{\phi}) \rangle = \prod_n \langle \exp(\hat{c}_n^\dagger(u_n^\dagger \lambda - \lambda^\dagger v_n^*) + \hat{c}_n(v_n^T \lambda - \lambda^\dagger u_n)) \rangle$ to the classical characteristic function $\chi_{classical}(\lambda, \lambda^*) = \langle \exp(\phi^\dagger \lambda - \lambda^\dagger \phi) \rangle = \prod_n \langle \exp(c_n^\dagger(u_n^\dagger \lambda - \lambda^\dagger v_n^*) + c_n(v_n^T \lambda - \lambda^\dagger u_n)) \rangle$. Thus the 2 characteristic functions agree if $\langle \exp(\hat{c}_n^\dagger \gamma + \hat{c}_n \gamma^*) \rangle = \langle \exp(c_n^* \gamma + \gamma^* c_n) \rangle = \frac{2}{\pi} \exp(-2|\gamma|^2)$